The FASEB Journal article fj.201600455RR. Published online August 26, 2016.

THE FASEB JOURNAL • RESEARCH • www.fasebj.org

# Intracellular alkalinization by phosphate uptake *via* type III sodium–phosphate cotransporter participates in high phosphate-induced mitochondrial oxidative stress and defective insulin secretion

**Tuyet Thi Nguyen,[*,†] Xianglan Quan,[*] Shanhua Xu,[*] Ranjan Das,[*] Seung-Kuy Cha,[*,‡] In Deok Kong,[*] Minho Shong,[§] Claes B. Wollheim,[¶] and Kyu-Sang Park[*,‡,1]**

[*]Department of Physiology and [‡]Mitohormesis Translational Research Center, Wonju College of Medicine, Yonsei University, Wonju, Korea; [†]Department of Physiology, Tan-Tao University College of Medicine, Long An, Vietnam; [§]Research Center for Endocrine and Metabolic Diseases, Chungnam National University School of Medicine, Daejeon, Korea; and [¶]Department of Cell Physiology and Metabolism, University of Geneva, Geneva, Switzerland

**ABSTRACT: Elevated plasma levels of inorganic phosphate ($P_i$) are harmful, causing, among other complications, vascular calcification and defective insulin secretion. The underlying molecular mechanisms of these complications remain poorly understood. We demonstrated the role of $P_i$ transport across the plasmalemma on $P_i$ toxicity in INS-1E rat clonal β cells and rat pancreatic islet cells. Type III sodium–phosphate cotransporters ($NaP_i$) are the predominant $P_i$ transporters expressed in insulin-secreting cells. Transcript and protein levels of PiT-1 and -2, isotypes of type III $NaP_i$, were upregulated by high $P_i$ incubation. In patch-clamp experiments, extracellular $P_i$ elicited a $Na^+$-dependent, inwardly rectifying current, which was markedly reduced under acidic extracellular conditions. Cellular uptake of $P_i$ elicited cytosolic alkalinization; intriguingly, this pH change facilitated $P_i$ transport into the mitochondrial matrix. Increased mitochondrial $P_i$ uptake accelerated superoxide generation, mitochondrial permeability transition, and endoplasmic reticulum stress-mediated translational attenuation, leading to reduced insulin content and impaired glucose-stimulated insulin secretion. Silencing of PiT-1/-2 prevented $P_i$-induced superoxide generation and mPT, and restored insulin secretion. We propose that $P_i$ transport across the plasma membrane and consequent cytosolic alkalinization could be a therapeutic target for protection from $P_i$ toxicity in insulin-secreting cells, as well as in other cell types.—Nguyen, T. T., Quan, X., Xu, S., Das, R., Cha, S.-K., Kong, I. D., Shong, M., Wollheim, C. B., Park, K.-S. Intracellular alkalinization by phosphate uptake *via* type III sodium–phosphate cotransporter participates in high phosphate-induced mitochondrial oxidative stress and defective insulin secretion. FASEB J. 30, 000–000 (2016). www.fasebj.org**

**KEY WORDS: inorganic phosphate · pancreatic β cells · mitochondrial permeability transition · endoplasmic reticulum stress · superoxide**

Inorganic phosphate ($P_i$) is an essential constituent in our body (1) and plays important biologic functions, including signal transduction and energy metabolism (2–6). $P_i$ is an indispensable cosubstrate for ATP synthesis in oxidative phosphorylation, which regulates insulin secretion in pancreatic β cells. The plasma $P_i$ concentration is tightly regulated in the range of 2.5 to 4.5 mg/dl (0.8–1.5 mM) by the gastrointestinal tract, the parathyroid gland, bone, and kidney (7, 8). The $P_i$ demand of body is recommended as between about 580 and 700 mg daily, which is mainly provided by the diet (9). However, a Western diet supplies about 1500 mg $P_i$ daily—almost twice the daily requirement (9). Accumulating evidence reveals that increasing $P_i$ induces apoptosis in endothelial cells (10), injury of podocytes (11), and transdifferentiation of vascular smooth muscle cells into bonelike cells. The latter may explain the underlying mechanism leading to Mönckeberg sclerosis in chronic kidney disease patients (8, 12). Prospective cohort studies showed that even in individuals with nonchronic kidney disease, plasma $P_i$ concentrations in the high normal

**ABBREVIATIONS:** AM, acetoxymethyl ester; BCECF, 2′,7′-*bis*-(2-carboxyethyl)-5-(and-6)-carboxyfluorescein; CCD, charge-coupled device; $\Delta\Psi_m$, mitochondrial membrane potential; eIF2α, α subunit of eukaryotic initiation factor; ER, endoplasmic reticulum; FBS, fetal bovine serum; GFP, green fluorescent protein; HEPES, 4-(2-hydroxyethyl)-1-piperazineethanesulfonic acid; KRB, Krebs–Ringer bicarbonate; mPT, mitochondrial permeability transition; MTT, (4,5-dimethylthiazol-2-yl)-2,5-diphenyltetrazolium bromide; $NaP_i$, sodium–phosphate cotransporter; NMDG, *N*-methyl-D-glucamine; PERK, double-stranded RNA-dependent protein kinase–like ER kinase; $pH_e$, extracellular pH; $pH_i$, intracellular pH; $pH_m$, mitochondrial matrix pH; $P_i$, inorganic phosphate; ROS, reactive oxygen species; siRNA, small interfering RNA; SBFI, sodium-binding benzofuran isophthalate; UPR, unfolded protein response

[1] Correspondence: Department of Physiology, Mitohormesis Translational Research Center, Wonju College of Medicine, Yonsei University, Ilsan-ro 20, Wonju, Gangwon-Do 26426, Korea. E-mail: qsang@yonsei.ac.kr

doi: 10.1096/fj.201600455RR

range (>3.5 mg/dl) correlates with cardiovascular events or mortality (8). Furthermore, individuals with elevated $P_i$ levels have an increased risk of impaired insulin secretion and the development of type 2 diabetes (13, 14).

Our previous work in insulin-secreting cells has demonstrated that high extracellular $P_i$ increases mitochondrial ROS generation and permeability transition pore opening, which lowers insulin content and attenuates glucose-stimulated insulin secretion (15). These results offer an explanation for earlier observations in Klotho mutant mice, with significantly higher plasma $P_i$ levels and reduced insulin synthesis compared to wild-type animals (16). Mitochondrial uptake of $P_i$ generates reactive oxygen species (ROS) as a consequence of an increased electrical gradient across the mitochondrial inner membrane. Mitochondrial oxidative stress induced by high $P_i$ perturbs endoplasmic reticulum (ER) calcium homeostasis and activates the unfolded protein response (UPR). Subsequent phosphorylation of the double-stranded RNA-dependent protein kinase–like ER kinase (PERK) and the α subunit of eukaryotic initiation factor (eIF2α) by high $P_i$ attenuate the translation of insulin (15). Inhibition of mitochondrial $P_i$ uptake and scavenging of mitochondrial ROS effectively abrogated the detrimental effects of high $P_i$—for example, restoring the reduced insulin content in pancreatic β cells (15).

Cellular $P_i$ uptake is mediated by type II and III sodium-dependent phosphate cotransporters ($NaP_i$) (17, 18). Type IIa and IIc $NaP_i$ are mainly expressed in renal tubules to reabsorb $P_i$ from urinary excretion, while type IIb is an important subtype for gastrointestinal $P_i$ absorption (19). Compared to type II $NaP_i$, type III $NaP_i$ (PiT-1 and -2) is found more ubiquitously and was suggested to play a housekeeping role in $P_i$ homeostasis (20). Intriguingly, PiT-1-dependent transport is also mediating detrimental effect of hyperphosphatemia such as injury of kidney podocyte and vascular calcification (11, 12, 21). We performed a study that demonstrated that plasmalemmal $P_i$ transport *via* PiT-1/-2 elicits cytosolic alkalinization, which further promotes $P_i$ uptake into mitochondria and accelerates ROS generation, leading to impaired insulin synthesis and secretion. Attenuation of $P_i$ transport either by acidic extracellular pH ($pH_e$) or silencing of the PiT-1/-2 transporters could protect β cells from high $P_i$-induced toxicity.

## MATERIALS AND METHODS

### Cell culture and isolation of pancreatic islets

Rat insulinoma INS-1E cells were cultured in a humidified atmosphere (37°C) containing 5% $CO_2$ in complete Roswell Park Memorial Institute (RPMI) 1640 medium (Thermo Fisher Scientific, Waltham, MA, USA) supplemented with 10% fetal bovine serum (FBS), 100 U/ml penicillin, 100 μg/ml streptomycin (Hyclone; Thermo Fisher Scientific), 1 mM sodium pyruvate, 50 μM 2-mercaptoethanol, 2 mM glutamine, and 10 mM 4-(2-hydroxyethyl)-1-piperazineethanesulfonic acid (HEPES; Sigma-Aldrich, St. Louis, MO, USA). HEK293 cells were cultured in complete DMEM (Hyclone).

Pancreatic islets were isolated from 200 to 300 g male Sprague Dawley rats (Orient Bio, Seongnam, Korea) with a modified protocol as described previously (22) by collagenase P (Sigma-Aldrich) digestion. The pancreas was then excised, digested, and dispersed at 37°C by a brief incubation with 0.25% trypsin-EDTA. Islet cells were seeded at a high density on 24-well plates coated with 804G matrix (23) ($3 \times 10^5$ cells per well) and cultured in RPMI 1640 medium supplemented with 10% FBS, 100 U/ml penicillin, and 100 μg/ml streptomycin (24). Animal experiments were approved by the Institutional Animal Care and Use Committee of Yonsei University–Wonju Campus.

### RT-PCR

Total RNAs were purified from trypsinized pellets of INS-1E cells and isolated pancreatic tissues. The first strand of cDNA was synthesized from 1 μg of total RNA using 50 U Moloney murine leukemia virus reverse transcriptase (Roche, Basel, Switzerland) by incubating for 1 h at 42°C. PCR conditions were as follows: 95°C for 5 min and 34 cycles of 94°C for 30 s, annealing at 58°C for 30 s, and 72°C for 45 s. Sequence-specific primers were used for $NaP_i$-IIa (forward: 5′-tgtcagcatggtctcctctg-3′, reverse: 5′-atgttgaaggaggcaaccac-3′), $NaP_i$-IIb (forward: 5′-cccatcattctgctgatcct-3′, reverse: 5′-ttttcctcctcctccaggtt-3′), $NaP_i$-IIc (forward: 5′-agactgctctgccatcacct-3′, reverse: 5′-gttaagcctgctccaacgag-3′), PiT-1 (forward: 5′-caaaagggagacgaaatgga-3′, reverse: 5′-agaagccatatgggtgttgc-3′), and PiT-2 (forward: 5′-ggatgggtatctgtggatgg-3′, reverse: 5′-atatgaaccaggaggcaacg-3′). Products were separated on 1.5% agarose gels and visualized by UV light.

Real-time PCR was performed to measure the mRNA levels of PiT-1/-2 using sequence-specific primers (forward: 5′-ccgtcagcaaccagatcaactc-3′ and reverse: 5′-cccatgcagtctcccaccttg-3′ for PiT-1, forward: 5′-ctattccaagaagaggctccg-3′ and reverse: 5′-tcaggatcggtcagctcag-3′ for PiT-2). β-Actin was used as the reference control. For the analysis of each gene expression, experiments were conducted in triplicate in a real-time PCR system (7900HT; Thermo Fisher Scientific) using SYBR Green PCR master mix (Qiagen, Germantown, MD, USA). The PCR reaction was performed with 10 μl total reaction volume containing 5 μl of 2× SYBR Green PCR master mix, 1 μl of 10 μM forward primer, 1 μl of 10 μM reverse primer, 1 μl of template cDNA (50 ng/μl), and 2 μl of DNase-RNase-free $H_2O$. In each PCR experiment, 40 cycles were considered, including denaturation at 95°C for 15 s, annealing at 58°C for 30 s, and extension at 72°C for 30 s. Data were analyzed following the $2^{-\Delta\Delta Ct}$ method.

### Western blot analysis

For total protein extraction, cells were lysed with cold radioimmunoprecipitation assay buffer (Thermo Fisher Scientific) containing protease inhibitor cocktail (Roche Diagnostics, Mannheim, Germany). The supernatant from lysates were loaded for SDS-PAGE and then transferred to PVDF membrane (EMD Millipore, Billerica, MA, USA). The membrane was blocked by 5% bovine serum albumin or 6% skim milk for 1 h at room temperature, followed by incubation with primary antibody at 4°C overnight. To detect the activation of ER stress markers, membranes were incubated with primary antibodies for phosphorylated and total PERK (1:1000, sc-32577, sc-13073; Santa Cruz Biotechnology, Santa Cruz, CA, USA) or eIF2α (1:1000, sc-101670, sc-133132; Santa Cruz Biotechnology). To estimate the protein levels of type III $NaP_i$, primary antibodies for PiT-1 (1:1000, 12423-I-AP; Proteintech Group, Chicago, IL, USA) and PiT-2 (1:1000, sc-68420; Santa Cruz Biotechnology) were used. β-Actin (1:5000, ab6276; Abcam, Cambridge, MA, USA) was used as a loading control. Horseradish peroxidase–conjugated secondary antibody against either mouse or rabbit IgG (31450, 31460, Thermo Fisher Scientific) was incubated for 1 h at room temperature. The bands were visualized with the UVP Biospectrum-600 imaging system using enhanced chemiluminescence solution (Luminata Forte; EMD Millipore).

### Electrophysiology experiments

HEK293 cells were cotransfected with PiT-1 and green fluorescent protein (GFP) plasmids together or only GFP plasmid as a control. PiT-1 plasmid was the kind gift of K. Hata (Osaka University, Japan). After 48 h, cells were split on poly-lysine-coated 12 mm coverslips for 4 to 6 h before recording. INS-1E cells were seeded on 804G matrix-coated 12 mm coverslips for 36 h before recording. Patch electrodes were fabricated from boroslicate glass capillary (Corning 8250; Garner Glass, Claremont, CA, USA). The electrodes were fire polished on a microforge and had a resistance of 1 to 3 MΩ when filled with the pipette solution. The cell membrane capacitance and series resistance were compensated over 80% electronically using an EPC-10 amplifier and Pulse/Pulsefit software (HEKA Electronik, Lambrecht, Germany). $P_i$-induced current was recorded when membrane potential was held at −100 mV. Bath solution included (in mM): 140 NaCl, 5 KCl, 10 HEPES, adjusted with NaOH to pH 7.4, osmolarity 300 to 310, adjusted by mannitol. Pipette solution included (in mM): 140 KCl, 10 HEPES, 1 $MgCl_2$, 10 EGTA, adjusted pH to 7.2 by KOH, osmolarity 298.

### Intracellular $Na^+$ measurement

To trace intracellular $Na^+$ changes by high $P_i$, the SBFI fluorescence dye (Molecular Probes, Eugene, OR, USA) was used. INS-1E cells seeded on 804G matrix-coated 12 mm coverslips ($3 \times 10^4$ cells) were loaded with sodium-binding benzofuran isophthalate, acetoxymethyl ester (SBFI-AM), 5 μM and sulfinpyrazone 250 μM in normal Krebs–Ringer bicarbonate (KRB) for 1 h at room temperature. After washout 2 times, cells were perfused with high $P_i$ (5 mM)-containing KRB solution (in mM: 140 NaCl, 3.6 KCl, 0.5 $NaH_2PO_4$, 0.5 $MgSO_4$, 1.5 $CaCl_2$, 10 HEPES, 2 $NaHCO_3$, 5.5 glucose). $Na^+$ calibration was performed as previously described (25). Briefly, $Na^+$ calibration solutions were made from a mixture of high $Na^+$ and high $K^+$ solution. The former include (in mM): 140 NaCl, 1.2 $CaCl_2$, 0.6 $MgCl_2$, and 10 HEPES. The latter was made by complete replacement of $Na^+$ by $K^+$. Fluorescence imaging of SBFI was performed by using an inverted microscope (IX-81; Olympus, Tokyo, Japan) equipped with a cooled charge-coupled device (CCD) camera (Cascade 512B; Photometrics, Tucson, AZ, USA). Cells were alternately excited at 340 nm and 380 nm by a light source (DG-4; Sutter, Novato, CA, USA), and images acquired at 510 nm were analyzed by Metafluor 6.3 software (Universal Imaging; Molecular Devices, Sunnyvale, CA, USA).

### Cytosolic pH measurement

INS-1E cells were seeded on 804G matrix-coated 18 mm coverslips ($3 \times 10^4$ cells) 36 h before the experiment. Cells were loaded with 2′,7′-*bis*-(2-carboxyethyl)-5-(and-6)-carboxyfluorescein, acetoxymethyl ester (BCECF-AM), 2.5 μM (Molecular Probes) and sulfinpyrazone 250 μM in 40 min at room temperature. After washout, cells were perfused with high $P_i$ (5 mM) and sulfinpyrazone (100 μM) containing KRB solution. Fluorescence imaging of BCECF (alternate excitation of 440 nm and 490 nm) were acquired at 540 nm and analyzed using Metafluor 6.3 software (Universal Imaging; Molecular Devices). Titration of pH was carried out by clamping the cytosolic pH with high $K^+$ buffers (in mM: 125 KCl, 5 NaCl, 1 $NaH_2PO4$, 1 $MgSO_4$, 10 HEPES) of defined pH containing nigericin (10 μM) and monensin (10 μM).

### Mitochondrial ROS measurement

Mitochondrial superoxide generation was determined using MitoSOX Red, a red fluorescence dye localized to mitochondria. Cells plated on 18 mm coverslips with $3 \times 10^4$ cells per well were treated with $P_i$ for the indicated time and then loaded with MitoSox Red 2.5 μM for 15 min at room temperature. Fluorescence images (excitation/emission: 510/580 nm) were obtained by using an inverted microscope with confocal spinning disk (CSU10; Yokogawa, Tokyo, Japan) and a cooled CCD camera. Data were analyzed by MetaMorph 6.3 software (Molecular Devices), which were from >3 independent experiments, >10 pictures from each, analyzing most cells in each picture.

### Mitochondrial matrix pH measurement

Mitochondrial matrix pH was measured using adenovirus expressing mtAlp$H_i$ (Ad-tetON-mAlp$H_i$) as described previously (24). At 72 h after transfection, fluorescence signals (excitation/emission: 488/535 nm) were recorded using the confocal microscope system described above. Titration of the mitochondrial pH was performed by clamping the matrix pH with high $K^+$ buffer (in mM: 125 KCl, 5 NaCl, 1 $NaH_2PO4$, 1 $MgSO_4$, 10 HEPES) of defined pH containing nigericin (10 μM) and monensin (10 μM) (26).

### Mitochondrial membrane potential measurement

JC-1 was used for the $\Delta\Psi_m$ measurements in permeabilized cells. Cells seeded on black-walled 96-well plates with $5 \times 10^4$ cells per well were loaded with JC-1 (500 nM) for 30 min at 37°C and then permeabilized with *Staphylococcus aureus* α toxin in intracellular buffer solution (in mM: 140 KCl, 5 NaCl, 7 $MgSO_4$, 1 $KH_2PO_4$, 1.65 $CaCl_2$, 10.2 EGTA, 20 HEPES, pH 7.0). The ratio of red (excitation/emission: 540/590 nm) over green (excitation/emission: 490/540 nm) fluorescence intensity was monitored from permeabilized cells with an intracellular buffer containing JC-1 (500 nM) using a multiwell fluorescence reader (FlexStation II; Molecular Devices) as previously described (27).

### Measurement of mitochondrial permeability transition pore opening

The opening of the mPT pore in intact cells can be traced directly by changes in calcein fluorescence as described previously (28, 29). Briefly, cells seeded on black-walled 96-well plates ($5 \times 10^4$ cells per well) were pretreated with or without $P_i$ for the indicated time and loaded with calcein-AM (1 μM) for 30 min at room temperature in the dark. Subsequently, after washout, cells were incubated with $CoCl_2$ (1 mM) for further 15 min at room temperature. Cells were washed again, and fluorescence intensity from calcein (excitation/emission: 485/530 nm) was monitored with a multiwell fluorescence reader (FlexStation II; Molecular Devices).

### Cell viability measurement

Cell viability was estimated by the MTT [(4,5-dimethylthiazol-2-yl)-2,5-diphenyltetrazolium bromide] colorimetric assay, which estimates the cellular reductive capacity (30). INS-1E cells were seeded on 804G matrix-coated 96-well plates with $5 \times 10^4$ cells per well, and $P_i$ was treated in DMEM (Hyclone) without FBS for 24 h. Then cells were incubated for 60 min at 37°C with thiazolyl blue tetrazolium bromide (Sigma-Aldrich); the absorbance ($A_{540}$) was measured by a microplate reader (Molecular Devices).

### Insulin measurement

To measure insulin content and secretion, cells seeded on 24-well plates were treated with 3 mM $P_i$ for 2.5 h in 2.8 mM glucose KRB solution. The cells were then incubated for 30 min at 37°C with 2.8

or 16.7 mM glucose KRB solution containing 0.1% bovine serum albumin (the different $P_i$ concentrations were maintained). The supernatant and cells extracted by the acid–ethanol were collected, and the level of insulin release and content were measured following the manufacturer's protocol with a rat insulin ELISA kit (Shibayagi, Gumma, Japan). The absorbance ($A_{450}$) was measured by a microplate reader (Molecular Devices).

### Small interfering RNA transfection

To knock down PiT-1/-2, SiGenome SmartPool small interfering RNA (siRNA) duplexes (mixture of 4 different siRNA targeting 4 different regions of 1 mRNA) were purchased from Bionner (Daejeon, Korea). Transfection of siRNA oligo was carried out using DharmaFECT-1 siRNA transfection reagent (T-2001-03; Thermo Fisher Scientific).

INS-1E cells ($3 \times 10^5$ cells per well) or dispersed pancreatic islet cells were plated on 804G matrix-coated 6-well plates for Western blot analysis or 24-well plates for insulin secretion assay, respectively, in penicillin-free medium. Transfection was carried out 1 h after plating according to the manufacturer's protocol, with minor variations. For a single 6-well or 24-well plate setting, total transfection volume was 2 ml or 500 μl, including 2.5 or 0.5 μl Dharmafect-1 and 100 nM siRNA, diluted in Opti-minimal essential medium (MEM) (31985-070; Thermo Fisher Scientific). In separate tubes, siRNA and Dharmafect-1 were diluted with Opti-MEM to a final volume of 200 or 50 μl in each tube and kept at room temperature. After 5 min, the contents of these 2 tubes were combined, pipetted out gently to mix, and kept for 20 min at room temperature. This step allowed the formation of the siRNA-transfection reagent complex that delivers siRNA into the cell. Antibiotic-free Opti-MEM (1.6 or 400 μl) was added to the cells grown in 35 or 15.6 mm dishes so that the final volume reached 2 ml or 500 μl. After 20 min, siRNA-transfection reagent complex was added by drops to the cells, with slow swirling to spread properly. Knockdown of genes was assessed at 48 h by determining mRNA levels using quantitative PCR. For assessing protein levels, Western blot analysis was performed at 72 h after siRNA transfection. Functional assays for siRNA-mediated gene silencing were performed at 48 h for mRNA level and 72 h for protein level after siRNA treatment.

### Statistical analysis

Values are presented as means ± SEM. *P* values were obtained by 2-tailed unpaired Student's *t* test or by 1- or 2-way ANOVA, followed by Turkey's multiple comparison test. $P < 0.05$ was considered to be statistically significant. Data analysis was performed by Prism 6 software (GraphPad Software, La Jolla, CA, USA).

## RESULTS

### PiT-1/-2 in INS-1E cells

In INS-1E cells and whole rat pancreatic tissue, higher expressions of PiT-1/-2 were detected at both the mRNA and protein level (**Fig. 1*A*, *B***). The transcriptional level of type II $NaP_i$ was undetectable in INS-1E cells, although there were higher expressions in rat kidney. When INS-1E cells were incubated in high $P_i$ concentration, PiT-1 mRNA level was

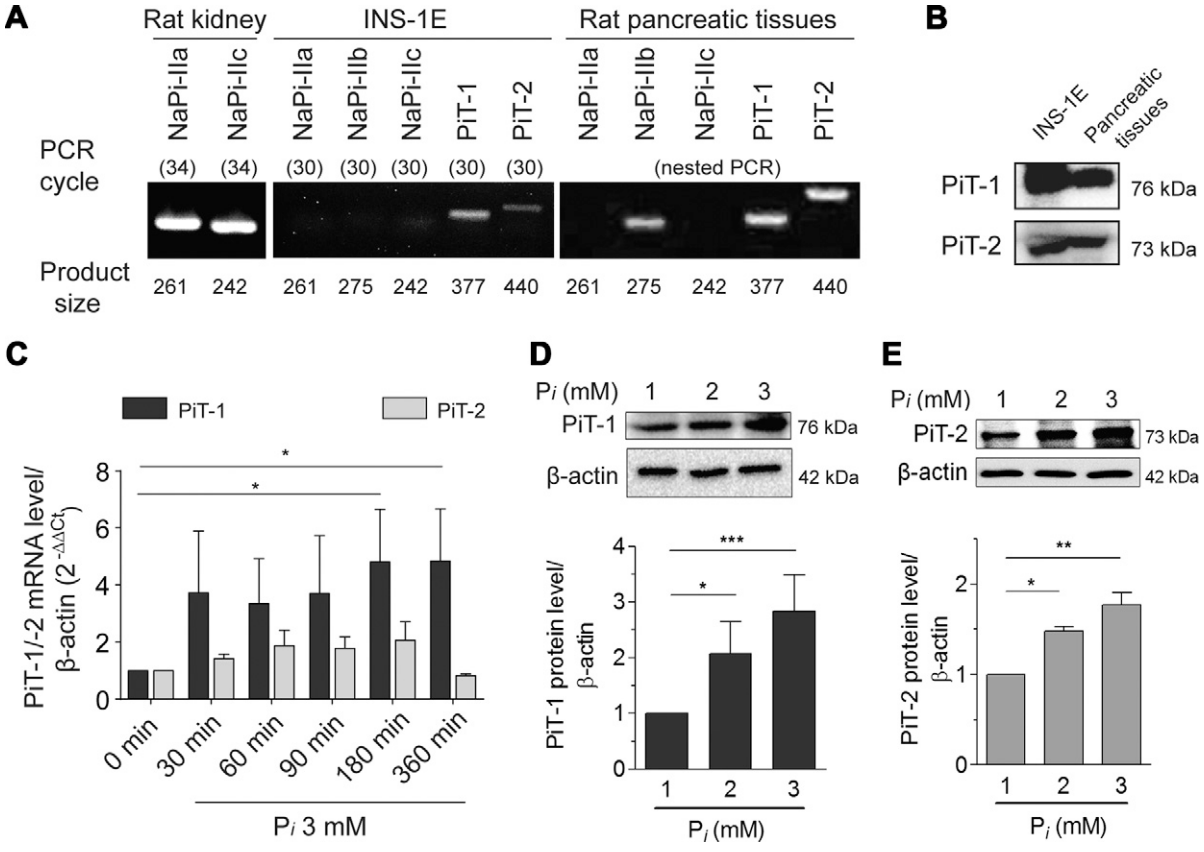


**Figure 1.** High $P_i$ up-regulates PiT-1/-2 in INS-1E cells. RT-PCR (*A*) and Western blot (*B*) analyses showed that PiT-1/-2 are abundantly expressed in INS-1E cells and rat pancreatic tissues. Transcript (*C*) and protein levels of PiT-1 (*D*), and PiT-2 (*E*) were up-regulated when INS-1E cells were exposed to high $P_i$ condition. $*P < 0.05$, $**P < 0.01$, and $***P < 0.001$.

significantly increased; PiT-2 mRNA level tended to increase without reaching significance (Fig. 1*C*). After 24 h incubation in high $P_i$–containing medium, the PiT-1/-2 proteins were also markedly up-regulated, which could further increase cellular $P_i$ uptake (Fig. 1*D*, *E*).

Patch clamp experiments were performed to characterize the $P_i$ transport in PiT-1-overexpressing HEK293 cells (**Fig. 2*A***). To measure the plasma membrane current when $P_i$ was applied, membrane voltage was clamped at −100 mV. $P_i$ induced an inward current in a dose-dependent manner (Fig. 2*B*). The membrane was held at −60 mV, and voltage pulses from −160 mV to −20 mV with 20 mV increments were applied. The $P_i$-induced current was strongly inwardly rectifying (Fig. 2*C*). This current disappeared when *N*-methyl-D-glucamine (NMDG) was used to substitute for $Na^+$ in the bath solution (Fig. 2*D*), demonstrating its exclusive dependence on extracellular $Na^+$. Interestingly, current density was markedly decreased at acidic pH (Fig. 2*E*, *F*). Similarly, in native INS-1E cells, the $P_i$-induced current required extracellular $Na^+$ (Fig. 2*G*) and showed similar pH dependence as in HEK293 cells (data not shown).

To directly demonstrate the $Na^+$ influx with $P_i$, we used SBFI as a cytosolic indicator of $Na^+$. Application of high $P_i$ increased the ratio of SBFI fluorescent intensities, which reflects intracellular $Na^+$ concentration in INS-1E cells (Fig. 2*H*).

## $P_i$-induced cytosolic alkalinization facilitates mitochondrial $P_i$ uptake

To study the alterations in intracellular pH ($pH_i$) by high $P_i$, BCECF was used to monitor $pH_i$. When the $pH_e$ was 7.4, basal $pH_i$ was increased from 7.16 to 7.73 by 5 mM $P_i$ (**Fig. 3*A***). At acidic $pH_e$ of 6.8, however, high $P_i$-induced cytosolic alkalinization was markedly reduced (Fig. 3*B*, *C*), consistent with the amplitude of inward currents. Mitochondrial $P_i$ uptake results in the hyperpolarization of the mitochondrial membrane potential ($\Delta\Psi_m$) (26). Interestingly, $P_i$-induced mitochondrial hyperpolarization had almost disappeared at an extramitochondrial pH ($pH_i$) of 6.6 in permeabilized cells. On the other hand, alkaline $pH_i$ strongly increased $\Delta\Psi_m$ hyperpolarization (Fig. 3*D*, *E*). We have shown previously that superoxide is generated as a result of mitochondrial $P_i$ uptake (15); therefore, the $pH_e$, through its effect on $P_i$ transport, may therefore influence $P_i$-induced ROS

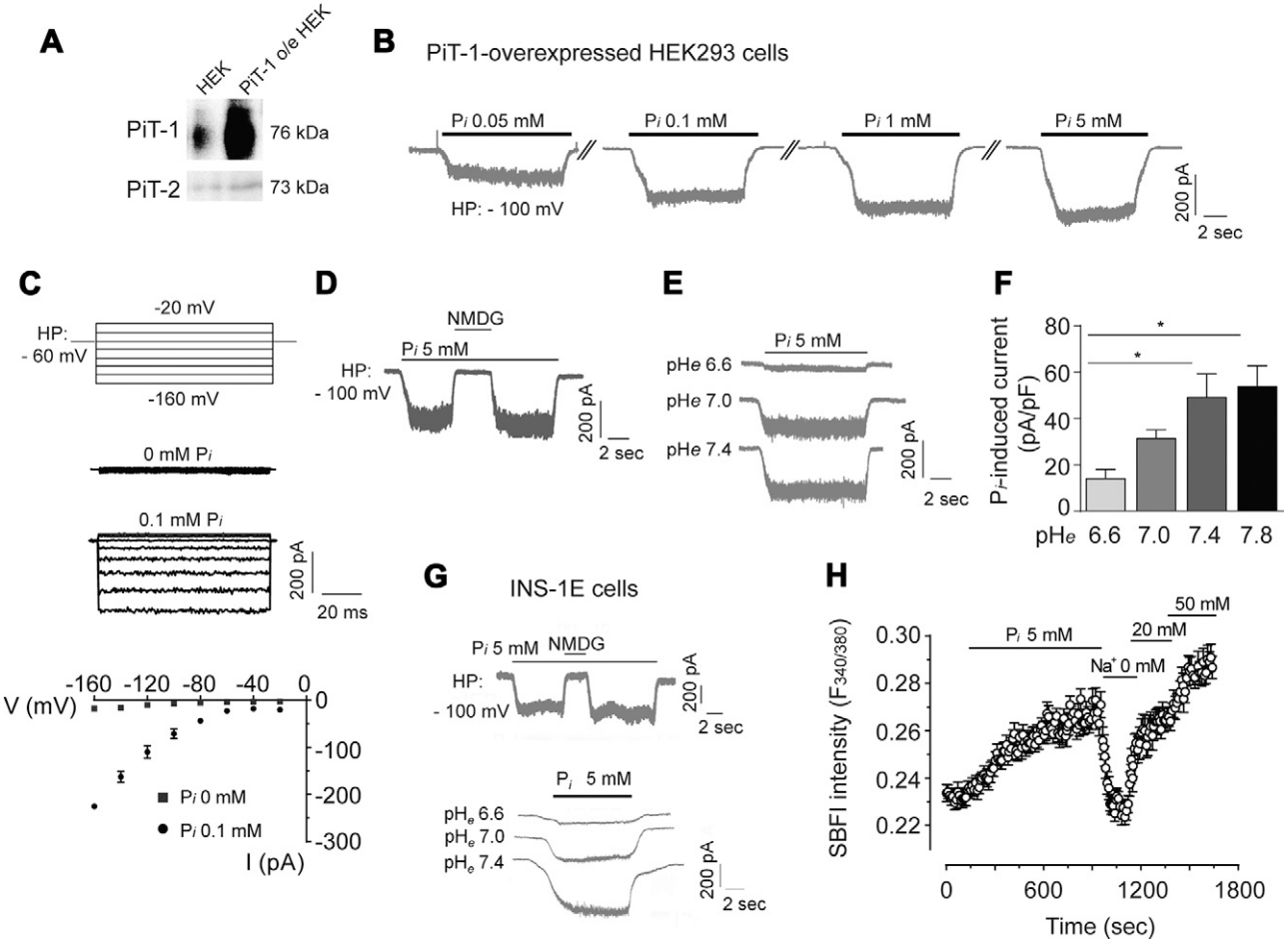


**Figure 2.** $P_i$ elicits inward currents and cytosolic $Na^+$ rise in dose- and pH-dependent manner. In PiT-1 overexpressed HEK293 cells (*A*), $P_i$ (0.05 ~ 5 mM) elicited dose-dependent inward currents clamped at −100 mV (*B*). This current showed inwardly rectifying characteristics (*C*), and extracellular $Na^+$ (*D*) and pH ($n = 4$; *E*, *F*) dependencies. In INS-1E cells, $P_i$ also induced $Na^+$-dependent inward currents with $pH_e$ dependencies (*G*). $P_i$ elevated increased intracellular $Na^+$ concentration measured by using $Na^+$ indicator SBFI-AM (*H*). $^*P < 0.05$.


 

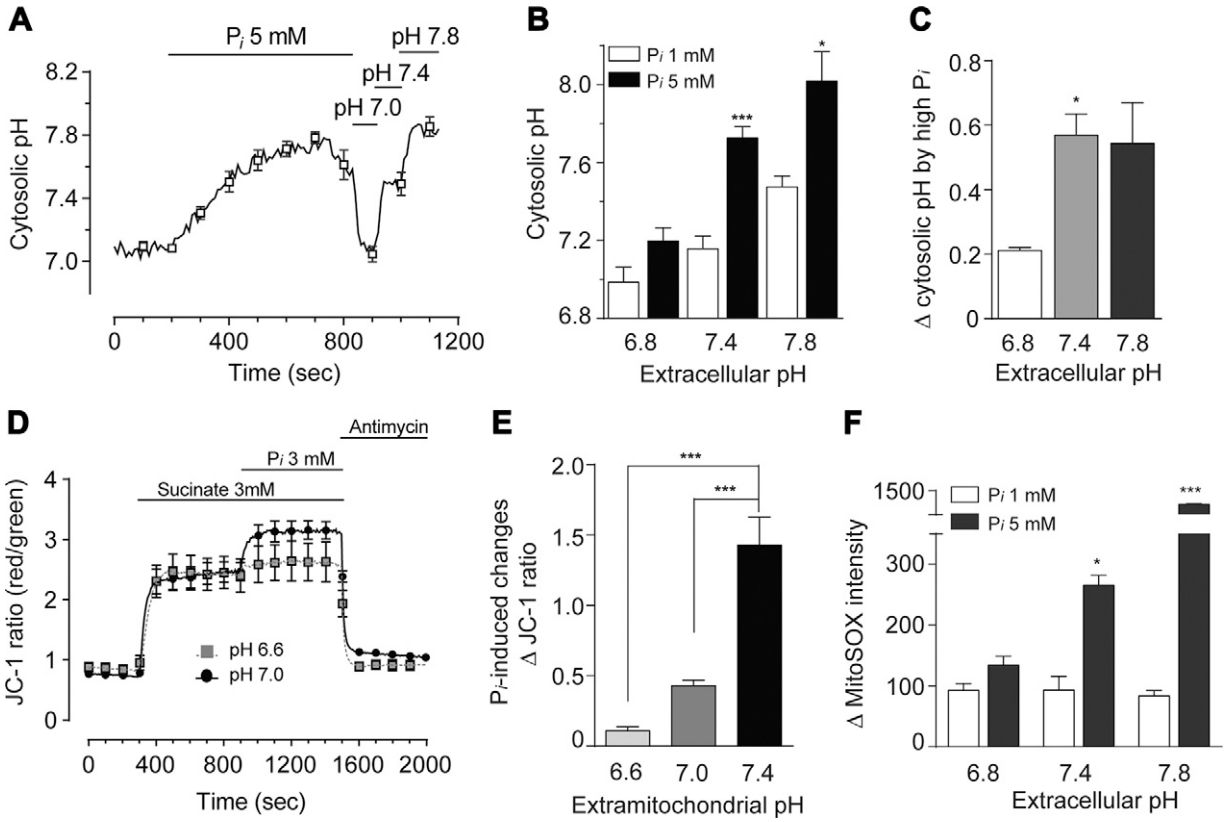


**Figure 3.** $P_i$ induces cytosolic alkalinization which facilitates mitochondrial $P_i$ uptake. $P_i$ induced intracellular alkalinization measured by using BCECF-AM, pH sensitive fluorescent dye ($n = 4$; *A*). Cytosolic alkalinization by high $P_i$ depended on $pH_e$ ($n = 3$–4; *B, C*). In permeabilized cells, $P_i$-induced hyperpolarization was significantly potentiated in alkaline extramitochondrial pH ($n = 6$; *D, E*). $P_i$-induced superoxide generation was also markedly elevated in extracellular alkaline conditions ($n = 4$; *F*). $^*P < 0.05$ and $^{***}P < 0.001$.

generation. Indeed, extracellular alkalinization strongly increased $P_i$-induced ROS production (Fig. 3*F*). These data indicate that mitochondrial $P_i$ uptake is potentiated in alkaline $pH_i$; thus, cytosolic alkalinization by cellular uptake of $P_i$ positively feeds forward to acceleration of $P_i$ transport into mitochondria and superoxide generation.

To test whether $P_i$ can alkalinize mitochondrial matrix pH ($pH_m$), which is known to stimulate mPT (31), we measured $pH_m$ by overexpression of mtAlpH*i* using adenovirus (27). High $P_i$ also alkalinized $pH_m$ (**Fig. 4*A***), which was abrogated by acidic $pH_e$ (Fig. 4*B, C*). Next, mPT pore opening was assessed using the calcein-$Co^{2+}$ quench technique (15). Calcein fluorescence was reduced when INS-1E cells were incubated in an elevated $P_i$ condition in a dose-dependent manner (Fig. 4*D*). The opening of the mPT pore was aggravated in the alkaline condition (Fig. 4*E*). Reductive capacity and survival of INS-1E cell were measured using the MTT assay (16). While acidic condition protected the cells from $P_i$ toxicity, alkanalization strongly diminished cell viability (Fig. 4*F*).

## Knockdown of PiT-1/-2 prevents high $P_i$-induced ROS generation, ER stress, and defective insulin secretion

To confirm the critical role of $P_i$ transport across the plasma membrane leading to oxidative stress, mPT, and cell death, transfection with siRNA against PiT-1 or PiT-2 was performed. Knockdown of both PiT-1 and PiT-2 reduced mRNA levels by 50 and 66%, respectively (**Fig. 5*A***). There was a corresponding reduction of PiT-1/-2 protein levels by 42 and 38% respectively (Fig. 5*B*). Blocking $P_i$ transport across the plasma membrane by knockdown of PiT-1/-2 significantly reduced mitochondrial superoxide production (Fig. 5*C, D*), and prevented mPT pore opening (Fig. 5*E*) and cell death (Fig. 5*F*) induced by $P_i$.

Glucose-stimulated insulin secretion was impaired in INS-1E cells after exposure to 3 mM $P_i$ in a time-dependent manner (**Fig. 6*A***). Cellular insulin content also showed a decrease in high $P_i$-incubated cells (Fig. 6*B*). It has been suggested that ROS elicits ER stress, including the UPR, which is pathogenic in type 2 diabetes (32). Phosphorylation of the UPR markers PERK and eIF2α was observed in INS-1E cells after 1 h exposure to 3 mM $P_i$ (Fig. 6*C, D*). The $P_i$-induced UPR was time dependent and coincided with the reduction in insulin content.

To extend our findings on $P_i$-induced ROS-mediated UPR as well as reduction of insulin release and content, experiments were performed in primary rat islet cells. Dispersed pancreatic islet cells were transfected with siRNA against PiT-1/-2 (Fig. 6*E*). Consistent with the results in INS-1E cells, UPR was activated when the islet cells were cultured in the high $P_i$ condition. Blocking cellular $P_i$ uptake by knockdown of PiT-1/-2 suppressed

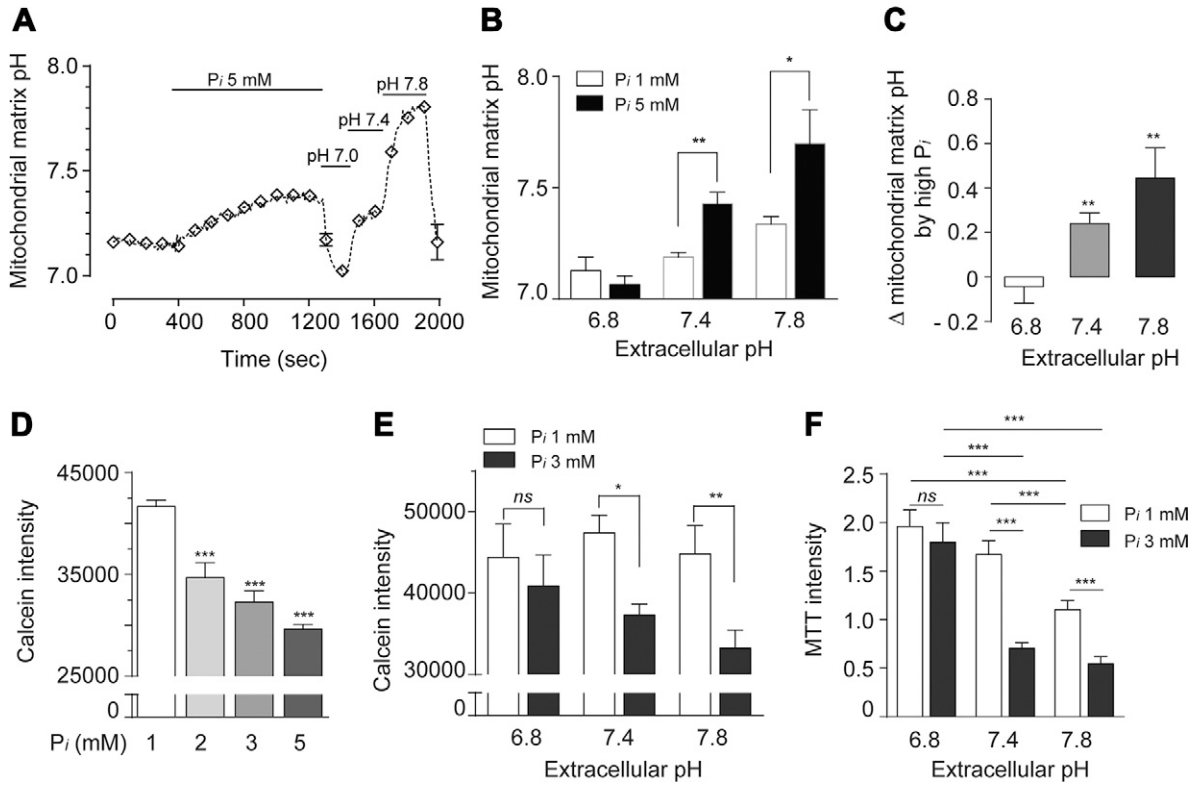


**Figure 4.** $P_i$ induces matrix alkalinization, mPT, and cell death in $pH_e$-dependent manner. Mitochondrial matrix pH was measured by infecting INS-1E cell with pH-sensitive florescent protein ($mtAlpH_i$)-encoded adenovirus (*A*). $P_i$ induced alkalinization of mitochondrial matrix, which depended on $pH_e$ ($n = 4$–6; *B, C*). $P_i$-induced mPT pore opening was detected by calcein-$Co^{2+}$ quench technique (*D*). Opening of mPT pore ($n = 5$–7; *E*) and cell death ($n = 3$; *F*) by high $P_i$ were exacerbated in extracellular alkaline condition. $^*P < 0.05$, $^{**}P < 0.01$, and $^{***}P < 0.001$.

the phosphorylation of PERK and eIF2α (Fig. 6*F–H*). As expected, reducing $P_i$ transport across the plasma membrane prevented $P_i$-induced impairment of insulin secretion by high glucose (Fig. 6*I, J*). Knockdown of PiT-1/-2 also abrogated the attenuating effects of high $P_i$ on insulin content (Fig. 6*K*).

## DISCUSSION

The present work clarifies that cellular uptake of $P_i$ induces cytosolic alkalinization mediated by PiT-1/-2 as the main plasma membrane $P_i$ transporters of INS-1E and pancreatic islet cells. This cytosolic pH change facilitates mitochondrial $P_i$ transport, which leads to superoxide generation, translational attenuation of insulin by ER stress, and secretory defects by mitochondrial dysfunction. The underlying mechanisms of $P_i$-induced defective insulin secretion are schematized in **Fig. 7**.

The characteristics of the $P_i$ transport across the plasma membrane were investigated by performing patch clamp recordings. Application of $P_i$ in external solution elicited a strong inwardly rectifying current in a dose-dependent manner. $P_i$-induced current disappeared when $Na^+$ was replaced by NMDG. These data suggest that PiT-1 works as an electrogenic cotransporter for $Na^+$ and $P_i$. This contention is supported by the increase of intracellular $Na^+$ by high $P_i$. The functional properties of type III $NaP_i$ have been investigated in oocytes from *Xenopus laevis* overexpressing PiT-1/-2 (17, 20). We observed in this study that $P_i$-induced current is potentiated in alkaline $pH_e$ both in PiT-1 overexpressing HEK293 cells (Fig. 2*E*) and native INS-1E cells. $P_i$ in plasma exists in 2 forms, monovalent $H_2PO_4^-$ and divalent $HPO_4^{2-}$, depending on pH ($pH_e$) (4, 5, 8). Because of its pKa (7.2), $HPO_4^{2-}$ is more abundant in an alkaline condition than $H_2PO_4^-$. Of note, high extracellular $P_i$ alkalinized cytosolic pH ($pH_i$) (Fig. 3*A*). Because of more acidic $pH_i$ than $pH_e$, $HPO_4^{2-}$ entered into the cytosol easily binds $H^+$ and depletes cytosolic proton. At $pH_e$ 6.8, where $H_2PO_4^-$ is dominant, $P_i$-induced current and cytosolic alkalinization were negligible compared to those at pH 7.4 or 7.8. It has been reported recently that extracellular acidification by $NH_4Cl$ treatment attenuates $P_i$-induced vascular calcification (33). This protective effect of acidic $pH_e$ might be the result of reduced $P_i$ uptake into smooth muscle cells, which is consistent to our findings. Taken together, the present data reveal that PiT-1 may preferentially transport the divalent form of $P_i$ ($HPO_4^{2-}$), and cellular $P_i$ uptake is accelerated in alkaline extracellular condition.

It has previously been demonstrated that mitochondrial $P_i$ uptake is driven by the pH gradient. $P_i$ uptake therefore dissipates the chemical gradient but at the same time increases the electrical gradient under the maintained proton motive force (26). $P_i$ also facilitates oxidative phosphorylation as a result of activation of metabolic enzymes and respiratory chain activity, which can further

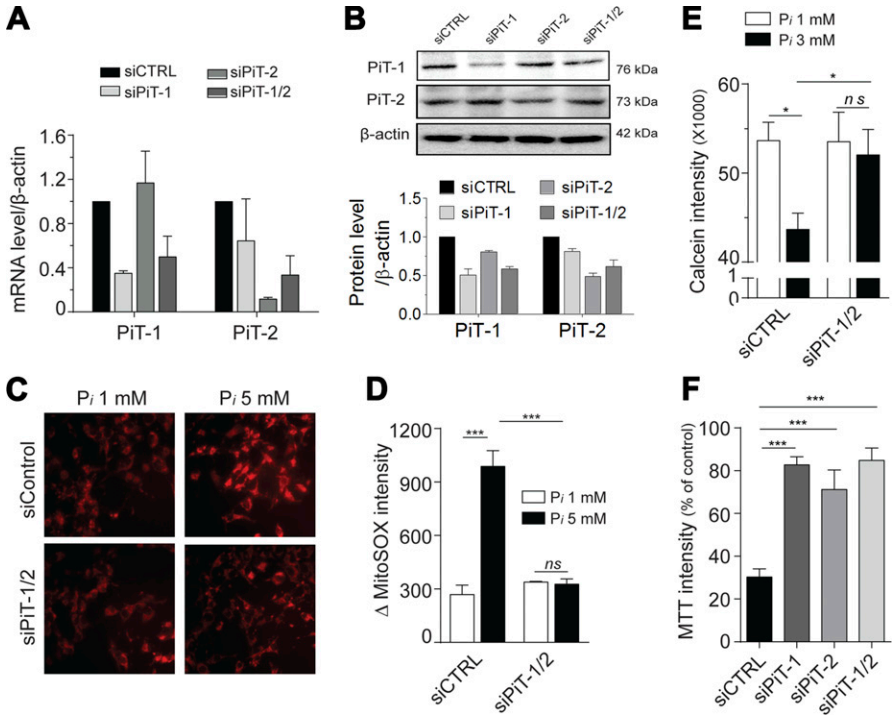


**Figure 5.** Knockdown of PiT-1/-2 blunted $P_i$-induced ROS generation, mPT pore opening, and prevented $P_i$-induced cell death. Quantitative PCR (*A*) and Western blot (*B*) analyses confirmed knockdown efficiency of siPiT-1/-2. $P_i$ (1 or 5 mM) was applied for 1 h. Double knockdown of PiT-1/-2 prevented ROS formation by $P_i$ (5 mM for 1 h) ($n = 3$; *C*, *D*), mPT pore opening ($n = 7$; *E*), and cell death ($n = 3$; *F*). $^*P < 0.05$ and $^{***}P < 0.001$.

elevate the $\Delta\Psi_m$ (34). The heightened electrical gradient by mitochondrial $P_i$ uptake causes increased ROS production. In particular, the present data demonstrate for the first time that $P_i$-induced hyperpolarization in alkaline extramitochondrial pH of permeabilized cells (the same as $pH_i$) is strikingly more marked than that under acidic conditions. These findings are interesting and consistent with the previous reports, in which the rate of ROS release was increased in mitochondrial matrix alkalinization. It has been suggested that the semiquinone radical ($SQ^-$) is stabilized by binding with protons, but lack of protons in mitochondrial matrix potentiates superoxide radical generation (35). Our findings suggest that acceleration of mitochondrial $P_i$ uptake by alkaline $pH_i$ could be another mechanism for ROS generation in response to alkaline condition. We also can infer that $P_i$ transports across the mitochondrial inner membrane also conduct mainly divalent form of $P_i$ similar to those of plasma membrane.

The mitochondrial permeability transition (mPT) pore has long been proposed to be a multiprotein complex

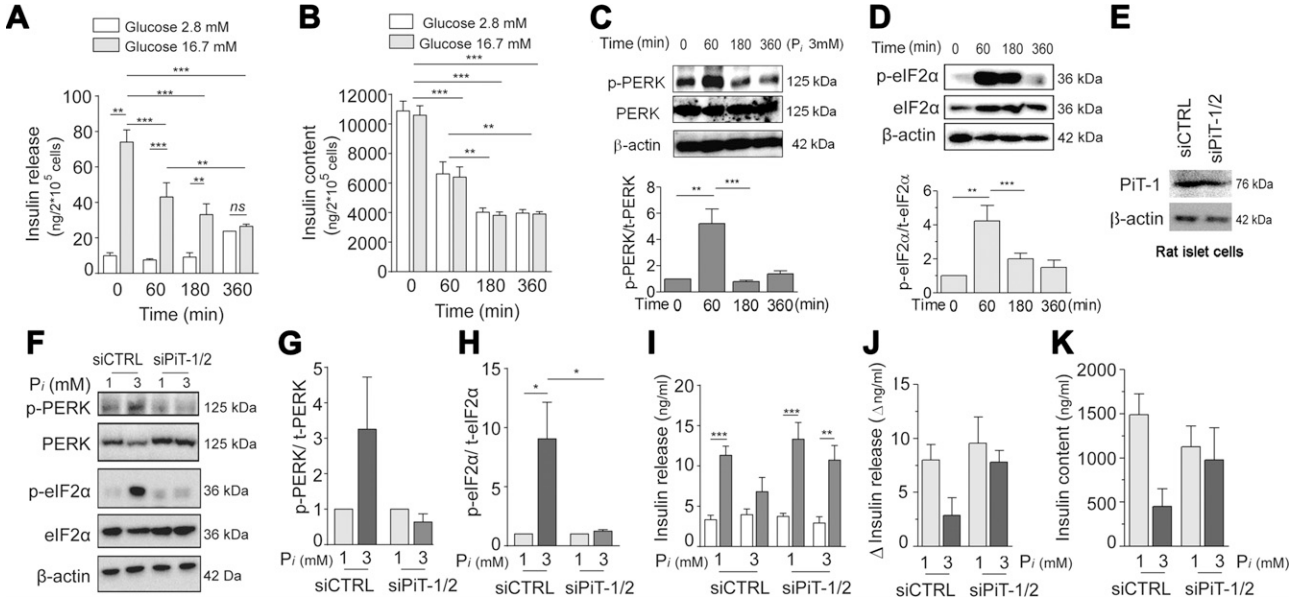


**Figure 6.** Knockdown of PiT-1/-2 prevented ER stress and restored defective insulin synthesis and secretion induced by high $P_i$. High extracellular $P_i$ impaired glucose-stimulated insulin secretion (GSIS, $n = 3$; *A*) and reduced insulin content ($n = 3$; *B*) in time-dependent manner. Incubation with 3 mM $P_i$ increased PERK (*C*) and eIF2α ($n = 3$; *D*). Reduced PiT-1 protein level in rat dispersed pancreatic islets by siPiT-1/-2 (*E*). Double knockdown of PiT-1/-2 prevented $P_i$-induced ER stress (*F*–*H*), impaired glucose-stimulated insulin secretion (*I*, *J*), and reduced insulin content (*K*). $^*P < 0.005$, $^{**}P < 0.01$, and $^{***}P < 0.001$.

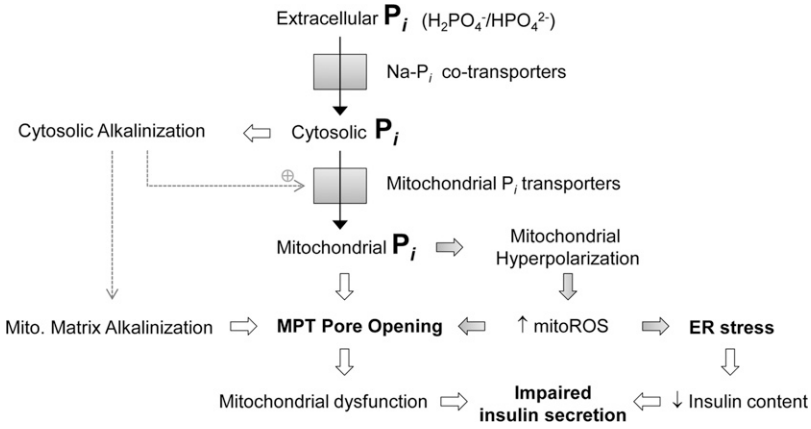


**Figure 7.** Proposed mechanisms of impaired insulin synthesis and secretion by high $P_i$ in pancreatic β cells.

composed of mitochondrial inner and outer membrane proteins, but molecular identification of its components has not yet been clearly elucidated (31, 36). Recent work by Alivian *et al.* (37) has provided evidence that the C subunit of ATP synthase could be a critical constituent of the mPT pore. The properties of the mPT pore vary depending on the tissue; for instance, the sensitivity to cyclosporine A is very low in mitochondria from brain or pancreatic β cells compared to those from other tissues (38). The factors regulating mPT pore opening include oxidative stress, adenine nucleotide depletion, pH, and mitochondrial matrix $Ca^{2+}$ or $P_i$ overload (31). These factors cooperate to increase permeability of the inner mitochondrial membrane, resulting in the loss of $\Delta\Psi_m$, mitochondrial swelling, and rupture of the outer mitochondrial membrane, causing release of proapoptotic intermembrane proteins into the cytosol. By using the calcein-$Co^{2+}$ quench technique, we observed higher permeability to $CoCl_2$ *via* mPT pore opening by $P_i$ in a dose-dependent manner. In addition, incubation of cells in acidic condition significantly reduced $P_i$-triggered mPT pore opening, contrasting with the drastic stimulation of mPT in alkaline pH. These data support the hypothesis that $P_i$-induced cytosolic alkalinization facilitates mitochondrial $P_i$ uptake, which increases the permeability of the mPT pore, exacerbating cell death. Blocking plasma membrane $P_i$ transport by knockdown of PiT-1/-2 completely suppressed ROS generation, inhibited mPT, and prevented cell death by high $P_i$ treatment. Therefore, we can infer that up-regulation of PiT-1/-2 by high $P_i$ incubation further exacerbates $P_i$ overload and consequent pathogenic changes, which could be a target for intervention to attenuate the following processes.

In prediabetes and diabetes, the β cells are exposed to high glucose concentrations. When blood glucose level is increased, the demand for insulin (a β cell produces 1 million proinsulin molecules per minute in response to hyperglycemic stimulation) poses a heavy burden on the ER (32). After folding of proinsulin in the ER, its processing to mature insulin is completed in the secretory granules. Proinsulin mRNA makes up as much as 20% of total β cell transcripts (39). Therefore, glucose-stimulated proinsulin translation may cause an excessive protein folding load on the ER, resulting in UPR and eventually ER stress (40). Our previous study revealed that mitochondrial $P_i$ uptake generates ROS, leading to ER stress and reduction of insulin content (15). In the present work, we found that high $P_i$ activates UPR, decreasing insulin content in a time-dependent manner. The defective insulin secretion and reduced hormone content evoked by high $P_i$ were prevented by knockdown of PiT-1/-2. We suggest that plasma membrane $P_i$ transport determines high $P_i$-induced β-cell toxicity, as depicted in Fig. 7.

We have shown that $P_i$ transported across the β-cell plasma membrane *via* PiT-1/-2 is taken up by the mitochondria. Subsequently, ROS generation correlates with the opening of the mPT pore, leading to mitochondrial dysfunction and defective insulin secretion. In addition, ROS production also initiates ER stress, causing UPR resulting in insulin translation attenuation, which lowers insulin content. These 2 mechanisms are proposed for the pathophysiological changes after β-cell exposure to high $P_i$ concentrations. It is proposed that the lowering of islet cell phosphate occurring during glucose-stimulated insulin secretion, referred to as the phosphate flush (41, 42), represents a protective mechanism to avoid phosphate cytotoxicity. Our results shed light on the harmful effects of hyperphosphatemia, evoked, among others, in the acceleration of the aging process. Inhibition of cellular $P_i$ uptake *via* PiT-1/-2, mitochondrial $P_i$ transporters, and the activation of the mitochondrial antioxidant system may be therapeutic approaches to treat phosphate toxicity with the potential of decreasing age-related metabolic diseases. FJ

## ACKNOWLEDGMENTS

This work was supported in part by a grant from the Korean National Research Foundation (NRF) funded by the Ministry of Science, Information and Communications Technology, and Future Planning (NRF-2014M3A9D8034464) (to M.S.).

## AUTHOR CONTRIBUTIONS

T. T. Nguyen, X. Quan, and K.-S. Park designed research; T. T. Nguyen, X. Quan, and S. Xu performed experiments and prepared figures; R. Das provided technical assistance; T. T. Nguyen and K.-S. Park wrote the manuscript; and S.-K. Cha, I. D. Kong, M. Shong, and C. B. Wollheim contributed to data analysis, discussions, and manuscript revision.

## REFERENCES


1. Penido, M. G., and Alon, U. S. (2012) Phosphate homeostasis and its role in bone health. *Pediatr. Nephrol.* **27**, 2039–2048
2. Takeda, E., Taketani, Y., Sawada, N., Sato, T., and Yamamoto, H. (2004) The regulation and function of phosphate in the human body. *Biofactors* **21**, 345–355
3. Hu, M. C., Kuro-o, M., and Moe, O. W. (2013) Renal and extrarenal actions of Klotho. *Semin. Nephrol.* **33**, 118–129
4. Kuro-o, M. (2013) A phosphate-centric paradigm for pathophysiology and therapy of chronic kidney disease. *Kidney Int Suppl (2011)* **3**, 420–426
5. Kuro-o, M. (2013) Klotho, phosphate and FGF-23 in ageing and disturbed mineral metabolism. *Nat. Rev. Nephrol.* **9**, 650–660
6. Takeda, E., Yamamoto, H., Nashiki, K., Sato, T., Arai, H., and Taketani, Y. (2004) Inorganic phosphate homeostasis and the role of dietary phosphorus. *J. Cell. Mol. Med.* **8**, 191–200
7. Razzaque, M. S. (2011) Phosphate toxicity: new insights into an old problem. *Clin. Sci.* **120**, 91–97
8. Gonzalez-Parra, E., Tunon, J., Egido, J., and Ortiz, A. (2012) Phosphate: a stealthier killer than previously thought? *Cardiovasc. Pathol.* **21**, 372–381
9. Jain, N., and Elsayed, E. F. (2013) Dietary phosphate: what do we know about its toxicity? *J. Nephrol.* **26**, 856–864
10. Di Marco, G. S., König, M., Stock, C., Wiesinger, A., Hillebrand, U., Reiermann, S., Reuter, S., Amler, S., Köhler, G., Buck, F., Fobker, M., Kümpers, P., Oberleithner, H., Hausberg, M., Lang, D., Pavenstädt, H., and Brand, M. (2013) High phosphate directly affects endothelial function by downregulating annexin II. *Kidney Int.* **83**, 213–222
11. Sekiguchi, S., Suzuki, A., Asano, S., Nishiwaki-Yasuda, K., Shibata, M., Nagao, S., Yamamoto, N., Matsuyama, M., Sato, Y., Yan, K., Yaoita, E., and Itoh, M. (2011) Phosphate overload induces podocyte injury *via* type III Na-dependent phosphate transporter. *Am. J. Physiol. Renal Physiol.* **300**, F848–F856
12. Crouthamel, M. H., Lau, W. L., Leaf, E. M., Chavkin, N. W., Wallingford, M. C., Peterson, D. F., Li, X., Liu, Y., Chin, M. T., Levi, M., and Giachelli, C. M. (2013) Sodium-dependent phosphate cotransporters and phosphate-induced calcification of vascular smooth muscle cells: redundant roles for PiT-1 and PiT-2. *Arterioscler. Thromb. Vasc. Biol.* **33**, 2625–2632
13. Fadda, G. Z., Hajjar, S. M., Perna, A. F., Zhou, X. J., Lipson, L. G., and Massry, S. G. (1991) On the mechanism of impaired insulin secretion in chronic renal failure. *J. Clin. Invest.* **87**, 255–261
14. Lorenzo, C., Hanley, A. J., Rewers, M. J., and Haffner, S. M. (2014) Calcium and phosphate concentrations and future development of type 2 diabetes: the Insulin Resistance Atherosclerosis Study. *Diabetologia* **57**, 1366–1374
15. Nguyen, T. T., Quan, X., Hwang, K. H., Xu, S., Das, R., Choi, S. K., Wiederkehr, A., Wollheim, C. B., Cha, S. K., and Park, K. S. (2015) Mitochondrial oxidative stress mediates high-phosphate-induced secretory defects and apoptosis in insulin-secreting cells. *Am. J. Physiol. Endocrinol. Metab.* **308**, E933–E941
16. Utsugi, T., Ohno, T., Ohyama, Y., Uchiyama, T., Saito, Y., Matsumura, Y., Aizawa, H., Itoh, H., Kurabayashi, M., Kawazu, S., Tomono, S., Oka, Y., Suga, T., Kuro-o, M., Nabeshima, Y., and Nagai, R. (2000) Decreased insulin production and increased insulin sensitivity in the Klotho mutant mouse, a novel animal model for human aging. *Metabolism* **49**, 1118–1123
17. Forster, I. C., Hernando, N., Biber, J., and Murer, H. (2012) Phosphate transport kinetics and structure–function relationships of SLC34 and SLC20 proteins. *Curr. Top. Membr.* **70**, 313–356
18. Werner, A., Dehmelt, L., and Nalbant, P. (1998) $Na^+$-dependent phosphate cotransporters: the NaPi protein families. *J. Exp. Biol.* **201**, 3135–3142
19. Miyamoto, K., Haito-Sugino, S., Kuwahara, S., Ohi, A., Nomura, K., Ito, M., Kuwahata, M., Kido, S., Tatsumi, S., Kaneko, I., and Segawa, H. (2011) Sodium-dependent phosphate cotransporters: lessons from gene knockout and mutation studies. *J. Pharm. Sci.* **100**, 3719–3730
20. Forster, I. C., Hernando, N., Biber, J., and Murer, H. (2013) Phosphate transporters of the SLC20 and SLC34 families. *Mol. Aspects Med.* **34**, 386–395
21. Li, X., Yang, H. Y., and Giachelli, C. M. (2006) Role of the sodium-dependent phosphate cotransporter, Pit-1, in vascular smooth muscle cell calcification. *Circ. Res.* **98**, 905–912
22. Massry, S. G. (2001) Insulin secretion in uremia. *Am. J. Kidney Dis.* **38** (4, Suppl 1)S58–S62
23. Parnaud, G., Bosco, D., Berney, T., Pattou, F., Kerr-Conte, J., Donath, M. Y., Bruun, C., Mandrup-Poulsen, T., Billestrup, N., and Halban, P. A. (2008) Proliferation of sorted human and rat beta cells. *Diabetologia* **51**, 91–100
24. Wiederkehr, A., Park, K. S., Dupont, O., Demaurex, N., Pozzan, T., Cline, G. W., and Wollheim, C. B. (2009) Matrix alkalinization: a novel mitochondrial signal for sustained pancreatic beta-cell activation. *EMBO J.* **28**, 417–428
25. Harootunian, A. T., Kao, J. P., Eckert, B. K., and Tsien, R. Y. (1989) Fluorescence ratio imaging of cytosolic free $Na^+$ in individual fibroblasts and lymphocytes. *J. Biol. Chem.* **264**, 19458–19467
26. Quan, X., Das, R., Xu, S., Cline, G. W., Wiederkehr, A., Wollheim, C. B., and Park, K. S. (2013) Mitochondrial phosphate transport during nutrient stimulation of INS-1E insulinoma cells. *Mol. Cell. Endocrinol.* **381**, 198–209
27. Quan, X., Nguyen, T. T., Choi, S. K., Xu, S., Das, R., Cha, S. K., Kim, N., Han, J., Wiederkehr, A., Wollheim, C. B., and Park, K. S. (2015) Essential role of mitochondrial $Ca^{2+}$ uniporter in the generation of mitochondrial pH gradient and metabolism-secretion coupling in insulin-releasing cells. *J. Biol. Chem.* **290**, 4086–4096
28. Petronilli, V., Miotto, G., Canton, M., Brini, M., Colonna, R., Bernardi, P., and Di Lisa, F. (1999) Transient and long-lasting openings of the mitochondrial permeability transition pore can be monitored directly in intact cells by changes in mitochondrial calcein fluorescence. *Biophys. J.* **76**, 725–734
29. Gautier, C. A., Giaime, E., Caballero, E., Núñez, L., Song, Z., Chan, D., Villalobos, C., and Shen, J. (2012) Regulation of mitochondrial permeability transition pore by PINK1. *Mol. Neurodegener.* **7**, 22
30. Janjic, D., and Wollheim, C. B. (1992) Islet cell metabolism is reflected by the MTT (tetrazolium) colorimetric assay. *Diabetologia* **35**, 482–485
31. Zorov, D. B., Juhaszova, M., Yaniv, Y., Nuss, H. B., Wang, S., and Sollott, S. J. (2009) Regulation and pharmacology of the mitochondrial permeability transition pore. *Cardiovasc. Res.* **83**, 213–225
32. Back, S. H., Kang, S. W., Han, J., and Chung, H. T. (2012) Endoplasmic reticulum stress in the β-cell pathogenesis of type 2 diabetes. *Exp. Diabetes Res.* **2012**, 618396
33. Leibrock, C. B., Alesutan, I., Voelkl, J., Pakladok, T., Michael, D., Schleicher, E., Kamyabi-Moghaddam, Z., Quintanilla-Martinez, L., Kuro-o, M., and Lang, F. (2015) NH4Cl treatment prevents tissue calcification in Klotho deficiency. *J. Am. Soc. Nephrol.* **26**, 2423–2433
34. Bose, S., French, S., Evans, F. J., Joubert, F., and Balaban, R. S. (2003) Metabolic network control of oxidative phosphorylation: multiple roles of inorganic phosphate. *J. Biol. Chem.* **278**, 39155–39165
35. Selivanov, V. A., Zeak, J. A., Roca, J., Cascante, M., Trucco, M., and Votyakova, T. V. (2008) The role of external and matrix pH in mitochondrial reactive oxygen species generation. *J. Biol. Chem.* **283**, 29292–29300
36. Halestrap, A. P., and Richardson, A. P. (2015) The mitochondrial permeability transition: a current perspective on its identity and role in ischaemia/reperfusion injury. *J. Mol. Cell. Cardiol.* **78**, 129–141
37. Alavian, K. N., Beutner, G., Lazrove, E., Sacchetti, S., Park, H. A., Licznerski, P., Li, H., Nabili, P., Hockensmith, K., Graham, M., Porter, G. A., Jr., and Jonas, E. A. (2014) An uncoupling channel within the c-subunit ring of the F1FO ATP synthase is the mitochondrial permeability transition pore. *Proc. Natl. Acad. Sci. USA* **111**, 10580–10585
38. Koshkin, V., Bikopoulos, G., Chan, C. B., and Wheeler, M. B. (2004) The characterization of mitochondrial permeability transition in clonal pancreatic beta-cells. Multiple modes and regulation. *J. Biol. Chem.* **279**, 41368–41376
39. Back, S. H., and Kaufman, R. J. (2012) Endoplasmic reticulum stress and type 2 diabetes. *Annu. Rev. Biochem.* **81**, 767–793
40. Scheuner, D., and Kaufman, R. J. (2008) The unfolded protein response: a pathway that links insulin demand with beta-cell failure and diabetes. *Endocr. Rev.* **29**, 317–333
41. Bukowiecki, L., Trus, M., Matschinsky, F. M., and Freinkel, N. (1979) Alterations in pancreatic islet phosphate content during secretory stimulation with glucose. *Biochim. Biophys. Acta* **583**, 370–377
42. Pierce, M., Freinkel, N., Dawson, R. M., Asplund, K., and Bukowiecki, L. (1978) 32P-labeling patterns in rat pancreatic islets: tissue source of the radiophosphate released after glucose stimulation. *Endocrinology* **103**, 971–977



*Received for publication March 21, 2016.*
*Accepted for publication August 8, 2016.*

# Intracellular alkalinization by phosphate uptake *via* type III sodium–phosphate cotransporter participates in high phosphate-induced mitochondrial oxidative stress and defective insulin secretion

Tuyet Thi Nguyen, Xianglan Quan, Shanhua Xu, et al.

*FASEB J* published online August 26, 2016
Access the most recent version at doi:10.1096/fj.201600455RR